after cratering events and catastrophic disruptions. The newly created object's orbits will gradually evolve and perhaps be transported into one of the strong resonances that can pump the orbit's eccentricity to Earth-crossing values. Smaller objects will migrate faster under the influence of the Yarkovsky effect[21], and once in a resonance the dynamical lifetime of objects of any size is of the order of only a few million years[2]. However, cosmic ray exposure ages tell us that most OC meteorites are tens of millions of years old[22]. This indicates that even the smallest meteoroids spend a considerable amount of time migrating from their point of origin into the resonances, and the larger objects that eventually become NEOs probably require even more time. Thus, we expect that NEOs of S-complex provenance will display a size-dependent range of spectra ranging from Q (or OC) to S. This prediction is supported by numerous reports in the past decade indicating Q-like spectra and a size-dependent trend to OC-like spectra with decreasing size in the NEO population[23–26]. However, space weathering in the main belt occurs faster than the lifetimes of NEOs, as suggested by meteoritic cosmic ray exposure ages[22]. Thus, observational evidence for a large number of OC-like spectra amongst the NEOs[23–26] implies that regular re-surfacing of these objects keep them looking younger longer. □

Received 21 October 2003; accepted 7 April 2004; doi:10.1038/nature02578.

1. Vokrouhlický, D. & Farinella, P. Efficient delivery of meteorites to the Earth from a wide range of asteroid parent bodies. *Nature* **407,** 606–608 (2000).
2. Gladman, B. J. *et al.* Dynamical lifetimes of objects injected into asteroid belt resonances. *Science* **277,** 197–201 (1997).
3. Wisdom, J. Meteorites may follow a chaotic route to earth. *Nature* **315,** 731–733 (1985).
4. Adams, J. B. & McCord, T. B. Alteration of lunar optical properties: Age and composition effects. *Science* **171,** 567–571 (1971).
5. Moroz, L. V., Fisenko, A. V., Semjonova, L. F., Pieters, C. M. & Korotaeva, N. N. Optical effects of regolith processes on S-asteroids as simulated by laser shots on ordinary chondrite and other mafic materials. *Icarus* **122,** 366–382 (1996).
6. Sasaki, S., Nakamura, K., Hamabe, Y., Kurahashi, E. & Hiroi, T. Production of iron nanoparticles by laser irradiation in a simulation of lunar-like space weathering. *Nature* **410,** 555–557 (2001).
7. Chapman, C. R. S-type asteroids, ordinary chondrites, and space weathering: The evidence from Galileo's fly-bys of Gaspra and Ida. *Meteorit. Planet. Sci.* **31,** 699–725 (1996).
8. Clark, B. E. *et al.* Space weathering on Eros: Constraints from albedo and spectral measurements of Psyche crater. *Meteorit. Planet. Sci.* **36,** 1617–1637 (2001).
9. Ivezić, Ž., Jurić, M., Lupton, R. H., Tabachnik, S. & Quinn, T. in *Survey and Other Telescope Technologies and Discoveries* (eds Tyson, J. A. & Wolff, S.) Vol. 4836, 98–103 *Proc. SPIE* (2002).
10. Hapke, B. Space weathering from Mercury to the asteroid belt. *J. Geophys. Res.* **106,** 10039–10074 (2001).
11. Michel, P., Benz, W., Tanga, P. & Richardson, D. C. Collisions and gravitational reaccumulation: Forming asteroid families and satellites. *Science* **294,** 1696–1700 (2001).
12. Milani, A. & Knežević, Z. Asteroid proper elements and the dynamical structure of the asteroid main belt. *Icarus* **107,** 219–254 (1994).
13. Gaffey, M. J. *et al.* Mineralogical variations within the S-type asteroid class. *Icarus* **106,** 573–602 (1993).
14. Doressoundiram, A., Barucci, M. A., Fulchignoni, M. & Florczak, M. EOS family: A spectroscopic study. *Icarus* **131,** 15–31 (1998).
15. Deeming, T. J. Stellar spectral classification, I. *Mon. Not. R. Astron. Soc.* **127,** 493–516 (1964).
16. Ivezić, Ž. *et al.* Color confirmation of asteroid families. *Astron. J.* **124,** 2943–2948 (2002).
17. Tedesco, E. F., Noah, P. V., Noah, M. & Price, S. D. The supplemental IRAS minor planet survey. *Astron. J.* **123,** 1056–1085 (2002).
18. Sykes, M. V. *et al.* The 2MASS asteroid and comet survey. *Icarus* **146,** 161–175 (2000).
19. Bus, S. J. & Binzel, R. P. Phase II of the small main-belt asteroid spectroscopic survey. *Icarus* **158,** 106–145 (2002).
20. Migliorini, F. *et al.* Surface properties of (6) Hebe: A possible parent body of ordinary chondrites. *Icarus* **128,** 104–113 (1997).
21. Morbidelli, A. & Vokrouhlický, D. The Yarkovsky-driven origin of near-Earth asteroids. *Icarus* **163,** 120–134 (2003).
22. Marti, K. & Graf, T. Cosmic-ray exposure history of ordinary chondrites. *Annu. Rev. Earth Planet. Sci.* **20,** 221–243 (1992).
23. Binzel, R. P., Bus, S. J., Burbine, T. H. & Sunshine, J. M. Spectral properties of near-Earth asteroids: evidence for sources of ordinary chondrite meteorites. *Science* **273,** 946–948 (1996).
24. Rabinowitz, D. L. Size and orbit dependent trends in the reflectance colours of earth-approaching asteroids. *Icarus* **134,** 342–346 (1998).
25. di Martino, M., Manara, A. & Migliorini, F. 1993 VW: an ordinary chondrite-like near-Earth asteroid. *Astron. Astrophys.* **302,** 609–612 (1995).
26. Lazzarin, M., di Martino, M., Barucci, M. A., Doressoundiram, A. & Florczak, M. Compositional properties of near-Earth asteroids: spectroscopic comparison with ordinary chondrite meteorites. *Astron. Astrophys.* **327,** 388–391 (1997).
27. Gaffey, M. J. Spectral reflectance characteristics of the meteorite classes. *J. Geophys. Res.* **81,** 905–920 (1976).

Supplementary Information accompanies the paper on **www.nature.com/nature**.

Acknowledgements We thank C. Chapman and J. Taylor for providing background on the S-complex conundrum and B. Clark for useful discussions and further studies. D.N. thanks NASA PG&G and the SwRI Quicklook programmes for providing support. Funding for the creation and distribution of the SDSS Archive has been provided by the Alfred P. Sloan Foundation, the Participating Institutions, the National Aeronautics and Space Administration, the National Science Foundation, the US Department of Energy, the Japanese Monbukagakusho, and the Max Planck Society. The SDSS website is http://www.sdss.org/.

Competing interests statement The authors declare that they have no competing financial interests.

Correspondence and requests for materials should be addressed to R.J. (jedicke@ifa.hawaii.edu).

Tonks–Girardeau gas of ultracold atoms in an optical lattice

Belén Paredes[1], Artur Widera[1,2,3], Valentin Murg[1], Olaf Mandel[1,2,3], Simon Fölling[1,2,3], Ignacio Cirac[1], Gora V. Shlyapnikov[4], Theodor W. Hänsch[1,2] & Immanuel Bloch[1,2,3]

[1]*Max-Planck-Institut für Quantenoptik, D-85748 Garching, Germany*
[2]*Sektion Physik, Ludwig-Maximilians-Universität, Schellingstrasse 4/III, D-80799 Munich, Germany*
[3]*Institut für Physik, Johannes Gutenberg-Universität, D-55099 Mainz, Germany*
[4]*Laboratoire Physique Théorique et Modèles Statistique, Université Paris Sud, Bâtiment 100, 91405 Orsay Cedex, France, and Van der Waals-Zeeman Institute, University of Amsterdam, 1018 XE Amsterdam, The Netherlands*

Strongly correlated quantum systems are among the most intriguing and fundamental systems in physics. One such example is the Tonks–Girardeau gas[1,2], proposed about 40 years ago, but until now lacking experimental realization; in such a gas, the repulsive interactions between bosonic particles confined to one dimension dominate the physics of the system. In order to minimize their mutual repulsion, the bosons are prevented from occupying the same position in space. This mimics the Pauli exclusion principle for fermions, causing the bosonic particles to exhibit fermionic properties[1,2]. However, such bosons do not exhibit completely ideal fermionic (or bosonic) quantum behaviour; for example, this is reflected in their characteristic momentum distribution[3]. Here we report the preparation of a Tonks–Girardeau gas of ultracold rubidium atoms held in a two-dimensional optical lattice formed by two orthogonal standing waves. The addition of a third, shallower lattice potential along the long axis of the quantum gases allows us to enter the Tonks–Girardeau regime by increasing the atoms' effective mass and thereby enhancing the role of interactions. We make a theoretical prediction of the momentum distribution based on an approach in which trapped bosons acquire fermionic properties, finding that it agrees closely with the measured distribution.

The physics of ultracold one-dimensional (1D) Bose systems is very different from that of ordinary three-dimensional (3D) cold gases[1,2,4,5]. For example, by decreasing the particle density n, a usual 3D quantum many-body system becomes more ideal, whereas in a 1D Bose gas the role of interactions becomes more important. The reason is that at temperatures $T \rightarrow 0$, the kinetic energy of a particle at the mean interparticle separation is $K \propto n^2$ and it decreases with decreasing density n faster than the interaction energy per particle, $I \propto n$. The ratio of the interaction to kinetic energy, $\gamma = I/K$, characterizes the different physical regimes of the 1D quantum gas. For a large value of γ, the gas enters the Tonks–Girardeau (TG) regime, where the repulsion between particles strongly decreases the wavefunction at short interparticle distances.

Achieving such a TG regime and observing 'fermionization' of the 1D Bose system is a great challenge, and it is complementary to the current experiments in which bosonic properties are observed in fermionic quantum gases[6–9]. The 1D regime is obtained by tightly confining the particle motion in two directions to zero point oscillations[4,5,10]. It was first demonstrated in experiments with weakly interacting Bose-condensed trapped gases, where $\gamma \ll 1$ (see refs 11, 12). In ref. 13, a tight radial confinement was realized by using two-dimensional (2D) optical lattice potentials to create an array of 1D quantum gases. In later experiments with optical lattices[14,15] it has become possible to reach a 1D regime with $\gamma \approx 1$, that is, in between a weakly interacting 1D Bose condensed gas and a fermionized TG gas. So far, however, it has not been possible to bridge the last one or two orders of magnitude in γ that could bring the bosonic quantum gas fully into the TG regime. Larger values of γ could either be reached by decreasing the density of the quantum gas or by increasing the effective interaction strength between the particles[4,5].

In this work, we propose and demonstrate a novel way to achieve the TG regime. The main point is to include an additional optical lattice along the 1D gas, which results in an increase of γ. For a homogeneous gas, γ can be expressed as $\gamma = mg/\hbar^2 n$, where g is the 1D interaction strength, m the mass of a single atom, and $\hbar$ denotes Planck's constant divided by 2π. The addition of a periodic potential along the third axis increases the effective mass, and thus leads to an increase of γ. In fact, in the limit in which only the first Bloch band is occupied, we have $I = U\nu$ and $K = J\nu$, where ν is the filling factor, U the on-site interaction energy and J the tunnelling amplitude, and thus $\gamma = U/J$. Additionally, in order to achieve a pure TG regime in a lattice, the filling factor ν should be smaller than unity: otherwise, doubly occupied sites would be present, and the direct correspondence to the TG gas would be lost (as in a recent experiment, see ref. 16). Following these ideas, we have been able to enter the TG regime with $\gamma \approx 5$–200. In this regime, the bosons can be theoretically described using a 'fermionization' approach[17,18].

For $\gamma \to \infty$, the ground state of N bosons at zero temperature is described by the many-body wavefunction:

$$\Psi_0(x_1, x_2, \ldots, x_N) \propto |\det[\varphi_i(x_j)]|, \quad i,j = 1,2,\ldots,N \qquad (1)$$

where det denotes the Slater determinant, and $\varphi_i(x)$ is the ith eigenfunction of the single-particle hamiltonian. The presence of the Slater determinant guarantees that the wavefunction vanishes whenever two particles occupy the same position in space. However, the absolute value of the determinant ensures that the wavefunction for the bosons remains completely symmetric. This wavefunction reflects the fundamental similarities between strongly interacting bosons and non-interacting fermions in one dimension, with properties such as the spatial density distribution, the density–density correlation function, or the entropy of the gas being the same as in the case of non-interacting fermions. More interestingly though, several properties are strongly modified by the presence of the absolute value of the determinant, leading to a unique behaviour of, for example, the momentum distribution of the TG gas[3]. This can be understood qualitatively in the following way: the bosonic particles in a TG gas are not allowed to occupy the same position in space. Owing to this restriction, they are distributed over a more extended region in momentum space than in the case of an ideal or weakly interacting Bose gas. On the other hand, in order to keep themselves apart from each other, they do not need to be in different momentum states, as would be the case for fermions.

We first describe the experimental realization together with the measured data, and then provide a detailed theoretical analysis of the system. In order to reach the regime of low filling factor, we start with a rather small Bose–Einstein condensate (BEC) of approximately $(3–4) \times 10^4$ ^{87}Rb atoms in a magnetic trap. Then the BEC is loaded into a 2D optical lattice potential (along the y- and z-axes), such that an array of 1D quantum gases confined to narrow potential tubes is created (Fig. 1a). The lattice potential is formed by superimposing two orthogonal standing waves with a wavelength of 823 nm on top of the BEC. In order to transfer the atoms into the optical potential, the potential depth of the optical lattice is first gradually increased to a mean final value of 27 E_r (Fig. 1b). Here E_r is the recoil energy $\hbar^2k^2/2m$, with k describing the wave vector of the lattice laser light. During this ramp up of the lattice potentials, the tunnel coupling between the different 1D quantum gases decreases exponentially. This results in a decoupling of the quantum gases, such that particle exchange between different tubes is suppressed. For the maximum lattice depth, the gaussian shape of the laser beams (160 μm waist) leads to an axial harmonic confinement of the 1D gases with a trapping frequency of $\omega_{ax} \approx 2\pi \times 60$ Hz. This has been verified by exciting a 'sloshing' motion of the thermal cloud and by parametric heating measurements, which both agree with the calculated value. Furthermore, the depths of all standing-wave potentials have been measured by vibrational band spectroscopy[19]. For such 1D quantum gases, without a lattice in the axial direction, we have $\gamma \approx 0.5$ near the lattice centre.

After a further hold time of 10 ms, we add an optical standing wave along the axial direction (x axis) in order to increase γ. The intensity of the laser forming this lattice potential (operated at a wavelength of 854 nm) is ramped up to a final depth V_{ax} of up to 18.5 E_r. The axial momentum distribution of the quantum gases is subsequently probed by suddenly removing all optical and magnetic trapping potentials, and by imaging the atom clouds after a time-of-flight period of 16 ms. In order to prevent a strong expansion of the atom cloud along the propagation axis of the imaging laser beam (z axis), which would make the experiment more sensitive to misalignments in the imaging axis, we reduce the confinement along this axis by lowering the z-lattice potential to 6 E_r within a time of 100 μs before initiating the ballistic expansion sequence. Also, along the x axis we use a ramp down, which is not fully non-adiabatic and leads to a narrowing of the gaussian envelope in the observed momentum distribution by ~20%. This enhances the number of atoms in the central momentum peak. From the

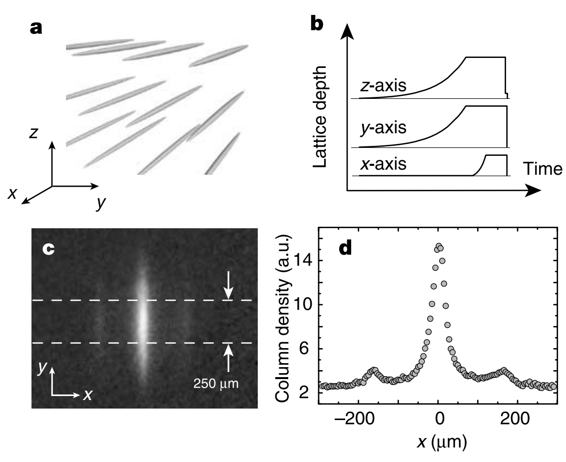

Figure 1 Experimental sequence and momentum profiles. **a**, Using a 2D optical lattice potential, we realize an array of 1D quantum gases. **b**, These quantum gases are created by first increasing the optical lattice depths along the y and z axes in an exponential ramp over a time of 160 ms (time constant $t = 40$ ms) to a mean final value of 27 E_r. After a further hold time of 10 ms at this final lattice depth, we increase the optical lattice potential along the x axis within a time of 20 ms (time constant $t = 10$ ms) to a variable lattice depth V_{ax}. The quantum gases are then allowed to equilibrate for another 30 ms before we probe the momentum distribution as described in the text. **c**, Typical time-of-flight images after a ballistic expansion of the atom clouds over a time of 16 ms for an axial optical lattice depth $V_{ax} = 6.5\ E_r$. The white dashed lines denote the area from which averaged momentum profiles along the x axis are extracted (**d**).

absorption images, we extract profiles of the axial momentum distribution by averaging horizontal profiles through the centre of the atom cloud (Fig. 1c).

In Fig. 2, we show six experimentally measured momentum profiles (see Supplementary Information for all 12 momentum profiles), corresponding to different values of the axial optical lattice depth ($V_{ax}/E_r = 0$–18.5). In Fig. 2a there is no lattice present along the x axis, and thus no first-order diffraction peak appears. Here, the value of γ is ~0.5 at the trap centre. For the rest of the figures (Fig. 2b–f) we can use the relation $\gamma \approx U/J$ obtaining $\gamma \approx 5$–200, which indicates that the TG regime is entered rather rapidly when increasing the axial lattice depth. In Fig. 2b–f we also plot our theoretical predictions based on fermionization at finite temperature averaged over the different 1D tubes (see Methods). Apart from a normalizing factor for each experimental curve, only the atom number in the central tube is used as an overall adjustable parameter in this model. This atom number is, however, kept constant between different momentum profiles. The initial temperature for the lowest axial lattice depth $V_{ax} = 4.6\ E_r$ has been obtained through a finite temperature fit to the corresponding momentum profiles using our fermionization approach. From this initial temperature, the temperatures of the quantum gases at

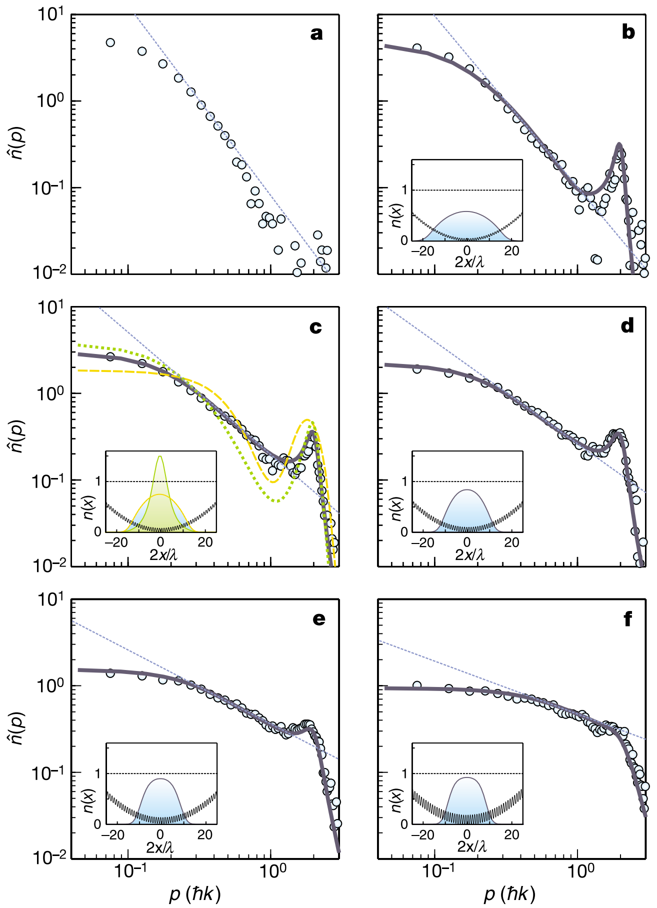

Figure 2 Momentum profiles of the 1D quantum gases for different axial lattice depths. In **b**–**f**, the experimental data (blue circles) are displayed together with our theoretical predictions (black line) based on fermionization at finite temperatures, averaged over the different 1D tubes. In order to emphasize the linear part of the momentum profiles, an auxiliary straight line with the corresponding slope is shown in each plot. In **c**, the momentum profiles for the ideal Bose gas (green dotted lines) and the ideal Fermi gas (yellow dashed lines) are also displayed for comparison. For all plots, an atomic distribution characterized by an atom number $N_{0,0} = 18$ in the central tube is used, for which we have found the best agreement with the experimental data (see Methods). In the insets of **b**–**f**, the density profile of a single 1D tube with $N = 15$ particles at the corresponding temperature and lattice depth is shown for the fermionized gas (black lines in plots **b**–**f**), for the ideal Fermi gas (yellow line in **c**), and for the ideal Bose gas (green line in **c**). The values of the axial lattice depths V_{ax}, the average temperatures, the slopes α of the linear part of the momentum profiles, and the values of $\gamma = U/J$ are: **b**, 4.6 E_r and $k_BT/J = 0.5$ (Tonks), $\alpha = 1.90$, $\gamma = 5.5$; **c**, 7.4 E_r and $k_BT/J = 0.7$ (Tonks), $k_BT/J = 1.6$ (ideal Bose gas), $k_BT/J = 0.7$ (ideal Fermi gas), $\alpha = 1.4$, $\gamma = 13.7$; **d**, 9.3 E_r and $k_BT/J = 0.9$ (Tonks), $\alpha = 1.2$, $\gamma = 23.6$; **e**, 12 E_r and $k_BT/J = 1.3$ (Tonks), $\alpha = 0.8$, $\gamma = 47.6$; and **f**, 18.5 E_r and $k_BT/J = 3.9$ (Tonks), $\alpha = 0.6$, $\gamma = 204.5$. For the momentum profile without the axial lattice (**a**), we find $\alpha = 2.2$ and $\gamma = 0.5$ at the centre of the trap.

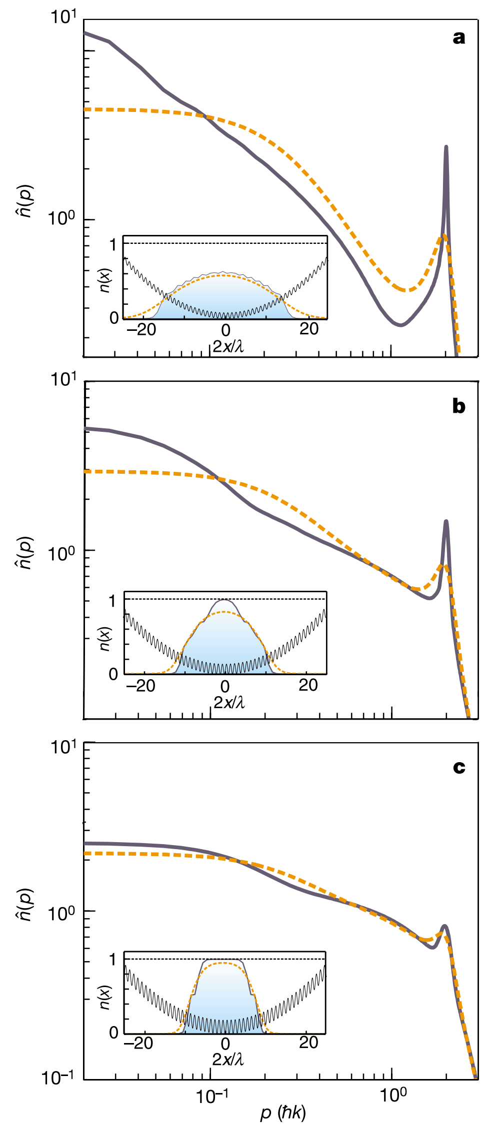

Figure 3 Momentum profiles of a single 1D tube obtained from our fermionization-based theory for different lattice depths. The plots are shown for axial lattice depths V_{ax} of 5.0 E_r (**a**), 9.5 E_r (**b**), and 12.0 E_r (**c**). For all plots, the number of particles is $N = 15$, and $b = 8 \times 10^{-4}\ E_r$ (this value of b corresponds to the trapping frequency of the experiment; see Methods). In each plot, the log–log momentum profile at $k_BT/J = 0$ (black line) is displayed together with that at $k_BT/J = 1.0$ (orange dashed line). The density profiles at $k_BT/J = 0$ and $k_BT/J = 1.0$, together with the corresponding lattice-harmonic potential, are shown in the inset of each plot. Note that at $k_BT/J = 0$, finite size effects make the slope at low momenta deviate from the ideal 1/2. The slope α is larger than 1/2 for small filling factors ($\alpha = 0.79$ in **a**), it approaches 1/2 as a Mott phase is developed at the centre of the trap ($\alpha = 0.49$ in **b**), and it decreases to zero deep in the Mott phase ($\alpha = 0.29$ in **c**).

increasing lattice depth $V_{\rm ax}$ have been modelled by assuming conservation of entropy during the ramp up of the axial lattice. For all 12 experimentally measured momentum profiles (see Supplementary Information), we find excellent agreement with the theory based on fermionization. For reference, we have plotted the results obtained assuming an ideal Bose or Fermi gas, also averaged over all the 1D tubes and at finite temperatures (see for example, Fig. 2c).

The observed momentum distributions allow us to conclude that we are dealing with a finite, non-uniform, TG gas in a lattice. Our results show pronounced deviations[20] from the generic behaviour of the uniform TG gas at zero temperature, where one has a $1/p^{1/2}$ low momentum distribution[3] giving a slope of 1/2 in the log–log plot. In our experiment we observe: (1) a rather flat momentum distribution at small momenta p, and (2) a linear region at larger p, with a slope decreasing with an increase in the lattice depth. This behaviour is in excellent agreement with the predictions of our fermionization-based theory for such a TG gas with a finite number of particles (about 20 per tube) in a lattice, in the presence of a harmonic trap, and at finite temperatures (see Fig. 3). Note that already for our lowest axial lattice depths we find $\gamma \gg 1$, and a further increase in the lattice depth mainly changes the average filling factor in our system and allows us to study the behaviour of a TG gas at different densities.

Most of the relevant physics concerning the momentum distribution for our case can be qualitatively understood by considering a uniform lattice system at the same temperature and with a filling factor equal to the average filling factor of the trapped system. We can then restrict the discussion to the case $\nu \leq 1/2$, because for $\nu > 1/2$ the system can be viewed as a system of holes at filling factor $1-\nu$. The filling factor determines a characteristic momentum $p_\nu = \hbar \times 2\pi\nu/\lambda$ related to the mean interparticle separation, where λ is the wavelength of the lattice laser light. At zero temperature, for $p \ll p_\nu$, the momentum distribution should exhibit a linear 1/2 behaviour, whereas for larger momenta short-range correlations[21] tend to increase the slope. An increase in the filling factor, and therefore a decrease in the average separation between particles, modifies p_ν and can therefore lead to a change of the observed slope. Note that for the case of $\nu = 1/2$, the momentum p_ν is the closest to the lattice momentum $\hbar \times 2\pi/\lambda$, and the momentum distribution is the least affected by short-range correlations. At finite temperatures a new momentum scale sets in[18,22], below which the slope has a tendency to decrease. This is the momentum $p_T = \hbar \times \pi/L_T$, where $L_T \approx \lambda J/k_{\rm B}T \sin\pi\nu$ is a characteristic length of thermal fluctuations. For a small filling factor, this length coincides with the gas phase result $L_T \approx \hbar^2 n/m^* k_{\rm B}T$, in which the particle mass is replaced by the effective mass $m^* = 2\hbar^2/J\lambda^2$. In our experiment we have $p_T \approx p_\nu$. Therefore, finite-temperature effects overlap with effects of short-range correlations and we observe a rather flat momentum distribution at small p, and a linear region with slope larger than 1/2 for larger p.

The presence of the harmonic trapping potential introduces important changes in the observed momentum profiles. First, in contrast to the uniform case, an adiabatic increase of the lattice depth increases the ratio $k_{\rm B}T/J$. This increases the momentum p_T, and the flat region extends to larger momenta. Second, the slope of the linear part decreases with the lattice depth, and the generic 1/2 value is recovered on approach to the Mott insulator transition[16,23–26]. This is a fundamental feature that is present irrespective of the number of particles and trap frequency. It is related to the fact that in the trapped case the characteristic average filling factor of the system increases with the lattice depth, because the tunnelling amplitude J decreases and particles try to accumulate near the trap centre. At the Mott insulator crossover, where the filling factor at the trap centre is equal to unity, the average filling factor is close to $\nu = 1/2$ (see Methods). This is the value for which the effects of short-range correlations are strongly suppressed in the homogeneous lattice system, and one comes closest to the generic behaviour with slope 1/2. Last, we note that in the weakly interacting regime for a trapped quasicondensate, one should have a lorentzian momentum distribution[27], which would give a slope close to 2 for $p \gg \hbar \times \pi/L_T$. Already, for low axial lattice depths $V_{\rm ax}$ we observe a smaller slope, which emphasizes a strong difference of our system from previously studied 1D quasicondensates.

In summary, we have prepared a TG gas in an optical lattice. Here the bosonic atoms exhibit a pronounced fermionic behaviour, and show a momentum distribution that is in excellent agreement with a theory of fermionized trapped Bose gases. In a next step, it will be intriguing to use photoassociation in optical lattices to probe the reduced two-body correlations, which are expected in a TG gas[28]. Furthermore, by using two bosonic atomic species and tuning the sign and strength of the atomic interactions, it should be possible to observe a behaviour similar to strongly correlated fermions. For example, the bosonic atoms can undergo a BCS transition and form Cooper pairs in the same way as electrons do in a superconductor[29]. □

Methods

Description of the 1D quantum gases using fermionization

Here we develop the theoretical treatment based on fermionization that we have used above to model the experiment. We consider N bosonic atoms moving in the lowest band of a 1D lattice and experiencing an additional harmonic potential. This situation is described by the Bose–Hubbard hamiltonian $H = H_{\rm B} + V$, where

$$H_{\rm B} = -J\sum_{\ell=-\infty}^{\infty}\left(a_\ell^\dagger a_{\ell+1} + a_{\ell+1}^\dagger a_\ell\right) + b\sum_{\ell=-\infty}^{\infty}\ell^2 a_\ell^\dagger a_\ell$$

$$V = U\sum_{\ell=-\infty}^{\infty} a_\ell^{\dagger 2} a_\ell^2$$

The term $H_{\rm B}$ describes the motion of the atoms in the combined lattice-harmonic potential, and the term V accounts for on-site interactions. The bosonic operators a_ℓ annihilate one boson at the ℓ th site, and fulfil canonical commutation relations $[a_\ell, a_{\ell'}^\dagger] = \delta_{\ell,\ell'}$. The parameter b is related to the frequency ω of the harmonic potential by $b = 1/8\, m\omega^2\lambda^2$.

We are interested in the strongly interacting or Tonks regime, in which two atoms cannot occupy the same lattice site. Within this regime, the bosonic operators a_ℓ can be re-expressed using the Jordan–Wigner transformation[30] (JWT) in terms of fermionic ones c_ℓ fulfilling $[c_\ell, c_{\ell'}^\dagger]_+ = \delta_{\ell,\ell'}$. Under the JWT, the interacting Bose hamiltonian $H_{\rm B}$ is transformed into a non-interacting fermionic hamiltonian $H_{\rm F}$ through the replacement $a_\ell \rightarrow c_\ell$. In order to predict the behaviour of the different bosonic observables, one has to transform them into fermionic ones via the JWT, and then evaluate the corresponding expectation values for the fermionic ground state. At $T = 0$, the fermionic ground state is given by the Slater determinant of equation (1). At a finite temperature T, the wavefunction is a mixture of different Slater determinants characterized by the many-body density matrix $\rho \propto \exp(-H_{\rm F}/k_{\rm B}T)$, where $k_{\rm B}$ is Boltzmann's constant.

Density and momentum distributions of fermionized Bose gases

The particle density $n(x)$ coincides with that of non-interacting fermions, as the JWT maps the corresponding bosonic observable onto the same fermionic one (that is $a_\ell^\dagger a_\ell \rightarrow c_\ell^\dagger c_\ell$). Under the Thomas–Fermi approximation we have:

$$n(x) = \frac{1}{\pi}\arccos\left(\max\left[\frac{\mu - bx^2}{-2J}, -1\right]\right)$$

if $\mu - bx^2 > -2J$ and zero otherwise. The size L of the cloud is $L = \lambda\sqrt{(2J+\mu)/4b}$, and μ is determined by imposing the condition that the total number of particles is N. When $\mu \geq 2J$ a Mott phase is produced at the centre of the trap, and $n(x=0)$ is equal to 1. At this point the average filling factor of the system $\bar\nu = \lambda N/2L \approx 3/\sqrt{2}\pi$, a value which is close to 1/2.

The momentum distribution $\hat n(p)$ is related to the one-particle correlation function $\langle a_\ell^\dagger a_{\ell'}\rangle$ through:

$$\hat n(p) = |\Phi(p)|^2 \sum_{\ell,\ell'=-\infty}^{\infty} e^{-ip(\ell-\ell')}\left\langle a_\ell^\dagger a_{\ell'}\right\rangle$$

where $\Phi(p)$ is the Fourier transform of the Wannier function, and p denotes momentum in units of $\hbar k$. Using the JWT, the bosonic one-particle correlation function can be re-expressed as:

$$\left\langle a_\ell^\dagger a_{\ell'}\right\rangle = \left\langle c_\ell^\dagger (-1)^{\sum_{\ell>m>\ell'} c_m^\dagger c_m} c_{\ell'}\right\rangle, \ell > \ell'$$

Making extensive use of Wick's theorem, one can re-express this quantity as a Töplitz determinant $\left\langle a_\ell^\dagger a_{\ell'}\right\rangle = \det[G_{\ell,\ell'}]$, where $G_{\ell,\ell'}$ is a $\ell-\ell'$, $\ell-\ell'$ matrix with elements $(G_{\ell,\ell'})_{x,y} = \left\langle c_{\ell'+y-1}^\dagger c_{\ell'+x}\right\rangle - \delta_{x,y-1}/2$.

Therefore, in order to evaluate the momentum distribution at a finite temperature T one has to determine the one-particle correlation functions for a non-interacting Fermi system at that temperature. We have used the grand canonical Fermi–Dirac distribution and the exact eigenstates $\varphi_i(x)$ of the single-particle hamiltonian to determine the momentum distribution in this way.

Averaging over the array of 1D quantum gases

In order to give a quantitative prediction for the experimental situation, we have averaged the momentum distribution for different tubes. To determine the atomic distribution, we have assumed that during the ramp up of the 2D optical lattice potential, tunnelling becomes negligible, and we have an array of independent 1D gases. For each tube, we have assumed a Thomas–Fermi density profile. Minimizing the total energy of the array with respect to the number of atoms in each of the tubes, we obtain $N_{i,j} = N_{0,0}\left(1 - \frac{5N}{2\pi N_{0,0}}(i^2 + j^2)\right)^{3/2}$, where $N_{i,j}$ is the number of atoms in a tube located at position (i, j) in the 2D optical lattice, N is the total number of particles in the array, and $N_{0,0}$ is the number of particles in the central tube. It follows that the probability of having a tube with M particles is:

$$P(M) = \frac{2}{3}\frac{1}{N_{0,0}^{2/3}M^{1/3}}, \quad M \le N_{0,0}.$$

Remarkably, this distribution only depends on one parameter, namely, the number of particles in the central tube, which is the only adjustable parameter in our model.

The temperature of each 1D quantum gas has been calculated assuming adiabatic evolution of the system during the ramp up of the axial lattice. Owing to the presence of the harmonic confinement, the ratio k_BT/J is not conserved in the adiabatic evolution. Given the temperature at $V_{ax} = 4.6\,E_r$ (see Supplementary Information), the conservation of entropy allows us to determine the temperature at the final lattice depth V_{ax}. The entropy of the TG gas coincides with that of the non-interacting Fermi gas, as both have the same spectrum and density of states. This results in the same temperatures for a TG gas and an ideal Fermi gas, but a different temperature for the ideal Bose gas when the axial lattice depth is increased. Note that tubes with different number of particles also have different temperatures at the same lattice depth.

Received 21 February; accepted 1 April 2004; doi:10.1038/nature02530.

1. Girardeau, M. Relationship between systems of impenetrable bosons and fermions in one dimension. *J. Math. Phys.* **1,** 516–523 (1960).
2. Lieb, E. H. & Liniger, W. Exact analysis of an interacting Bose gas. The general solution and the ground state. *Phys. Rev.* **130,** 1605–1616 (1963).
3. Lenard, A. Momentum distribution in the ground state of the one-dimensional system of impenetrable bosons. *J. Math. Phys.* **5,** 930–943 (1964).
4. Petrov, D. S., Shlyapnikov, G. V. & Walraven, J. T. M. Regimes of quantum degeneracy in trapped 1D gases. *Phys. Rev. Lett.* **85,** 3745–3749 (2000).
5. Dunjko, V., Lorent, V. & Olshanii, M. Bosons in cigar-shaped traps: Thomas-Fermi regime, Tonks-Girardeau regime, and in between. *Phys. Rev. Lett.* **86,** 5413–5416 (2001).
6. Jochim, S. *et al.* Bose-Einstein condensation of molecules. *Science* **302,** 2101–2103 (2003).
7. Greiner, M., Regal, C. & Jin, D. S. Emergence of a molecular Bose-Einstein condensate from a Fermi gas. *Nature* **426,** 537–540 (2003).
8. Zwierlein, M. W. *et al.* Observation of Bose-Einstein condensation of molecules. *Phys. Rev. Lett.* **91,** 250401 (2003).
9. Regal, C., Greiner, M. & Jin, D. S. Observation of resonance condensation of fermionic atom pairs. *Phys. Rev. Lett.* **92,** 040403 (2004).
10. Olshanii, M. Atomic scattering in the presence of an external confinement. *Phys. Rev. Lett.* **81,** 938–941 (1998).
11. Goerlitz, A. *et al.* Realization of Bose-Einstein condensates in lower dimensions. *Phys. Rev. Lett.* **87,** 130402 (2001).
12. Schreck, F. *et al.* A quasipure Bose-Einstein condensate immersed in a Fermi sea. *Phys. Rev. Lett.* **87,** 080403 (2001).
13. Greiner, M., Bloch, I., Mandel, O., Hänsch, T. W. & Esslinger, T. Exploring phase coherence in a 2D lattice of Bose-Einstein condensates. *Phys. Rev. Lett.* **87,** 160405 (2001).
14. Moritz, H., Stöferle, T., Köhl, M. & Esslinger, T. Exciting collective oscillations in a trapped 1D gas. *Phys. Rev. Lett.* **91,** 250402 (2003).
15. Laburthe Tolra, B., *et al.* Observation of reduced three-body recombination in a fermionized 1D Bose gas. Preprint at ⟨http://xxx.lanl.gov/cond-mat/0312003⟩ (2003).
16. Stöferle, T., Moritz, H., Schori, C., Köhl, M. & Esslinger, T. Transition from a strongly interacting 1D superfluid to a Mott insulator. *Phys. Rev. Lett.* **92,** 130403 (2004).
17. Efetov, K. B. & Larkin, A. I. Correlation functions in one-dimensional systems with strong interactions. *Sov. Phys. JETP* **42,** 390–396 (1976).
18. Korepin, V. E., Bogoliubov, N. M. & Izergin, A. G. *Quantum Inverse Scattering Method and Correlation Functions* (Cambridge Univ. Press, Cambridge, 1993).
19. Ovchinnikov, Y. B. *et al.* Diffraction of a released Bose-Einstein condensate by a pulsed standing light wave. *Phys. Rev. Lett.* **83,** 284–287 (1999).
20. Astrakharchik, G. E. & Giorgini, S. Correlation functions and momentum distributions of one-dimensional Bose systems. *Phys. Rev. A* **68,** 031602 (2003).
21. Olshanii, M. & Dunjko, V. Short-distance correlation properties of the Lieb-Liniger system and momentum distributions of trapped one-dimensional atomic gases. *Phys. Rev. Lett.* **91,** 090401 (2003).
22. Cazalilla, M. A. Bosonizing one-dimensional cold atomic gases. *J. Phys. B* **37,** S1–S47 (2004).
23. Fisher, M. P. A., Weichman, P. B., Grinstein, G. & Fisher, D. S. Boson localization and the superfluid-insulator transition. *Phys. Rev. B* **40,** 546–570 (1989).
24. Jaksch, D., Bruder, C., Cirac, J. I., Gardiner, C. W. & Zoller, P. Cold bosonic atoms in optical lattices. *Phys. Rev. Lett.* **81,** 3108–3111 (1998).
25. Greiner, M., Mandel, O., Esslinger, T., Hänsch, T. W. & Bloch, I. Quantum phase transition from a superfluid to a Mott insulator in a gas of ultracold atoms. *Nature* **415,** 39–44 (2002).
26. Kollath, C., Schollwöck, U., von Delft, J. & Zwerger, W. Spatial correlations of trapped one-dimensional bosons in an optical lattice. *Phys. Rev. A* **69,** 031601 (2004).
27. Richard, S. *et al.* Momentum spectroscopy of 1D phase fluctuations in Bose-Einstein condensates. *Phys. Rev. Lett.* **91,** 010405 (2003).
28. Gangardt, D. M. & Shlyapnikov, G. V. Stability and phase coherence of trapped 1D Bose gases. *Phys. Rev. Lett.* **90,** 010401 (2003).
29. Paredes, B. & Cirac, J. I. From Cooper pairs to Luttinger liquids with bosonic atoms in optical lattices. *Phys. Rev. Lett.* **90,** 150402 (2003).
30. Sachdev, S. *Quantum Phase Transitions* (Cambridge Univ. Press, Cambridge, 1999).

Supplementary Information accompanies the paper on **www.nature.com/nature**.

Acknowledgements We thank F. Gerbier, D. Gangardt and M. Olshanii for discussions, and M. Greiner for help in setting up the experiment. I.B. also acknowledges support from AFOSR.

Competing interests statement The authors declare that they have no competing financial interests.

Correspondence and requests for materials should be addressed to I.B. (bloch@uni-mainz.de).

Synthesis and characterization of chiral mesoporous silica

Shunai Che[1], Zheng Liu[2,3], Tetsu Ohsuna[3], Kazutami Sakamoto[4], Osamu Terasaki[3] & Takashi Tatsumi[5]

[1] *Department of Chemistry, School of Chemistry and Chemical Technology, Shanghai Jiao Tong University, 800 Dongchuan Road, Shanghai, 200240, China*
[2] *Bussan Nanotech Research Institute, 2-1 Koyadai, Tsukuba, Ibaraki 305-0074, Japan*
[3] *Structural Chemistry, Arrhenius Laboratory, Stockholm University, S-10691 Stockholm, Sweden*
[4] *AminoScience Laboratory, Ajinomoto Co., Inc., 1-1 Suzuki-cho, Kawasaki 210-8681, Japan*
[5] *CREST, JST, Division of Materials Science and Chemical Engineering, Faculty of Engineering, Yokohama National University, 79-5 Tokiwadai, Yokohama 240-8501, Japan*

Chirality is widely expressed in organic materials, perhaps most notably in biological molecules such as DNA, and in proteins, owing to the homochirality of their components (D-sugars and L-amino acids). But the occurrence of large-scale chiral pores in inorganic materials is rare[1]. Although some progress has been made in strategies to synthesize helical and chiral zeolite-like materials[1–3], the synthesis of enantiomerically pure mesoporous materials is a challenge that remains unsolved[4]. Here we report the surfactant-templated synthesis of ordered chiral mesoporous silica, together with a general approach for the structural analysis of chiral mesoporous crystals by electron microscopy. The material that we have synthesized has a twisted hexagonal rod-like morphology, with diameter 130–180 nm and length 1–6 μm. Transmission electron microscopy combined with computer simulations confirm the presence of hexagonally ordered chiral channels of 2.2 nm diameter winding around the central axis of the rods. Our findings could lead to new uses for mesoporous silica and other chiral pore materials in, for example, catalysis and separation media, where both shape selectivity and enantio-selectivity[5] can be applied to the manufacturing of enantiomerically pure chemicals and pharmaceuticals.

We recently discovered a templating route for preparing well-ordered mesoporous silicas based on the self-assembly of chiral anionic surfactants and inorganic precursors by using aminosilane or quaternized aminosilane as a co-structure-directing agent (CSDA)[6], which provided a potential method to synthesize mesoporous materials with inherent chirality. Among the anionic surfactants tested in our previous work, N-acyl-L-alanine is a chiral organic molecule that can form a chiral nematic phase in the presence of small amounts of decanol[7,8]. This phenomenon has